Suppporting Information

Achieving Ultrahigh Initial Coulombic Efficiency in SnBi/C Anode for Sodium-Ion Batteries via Interfacial Engineering and Binder Optimization

Chunting Wang, [a] Qian Yao, [b] Long Su,[c] Jingjing Dong, [a] Yingchun Yan,*[a] Weimin Zhang,[a] and Jian Yang*[b]

[a] *School of Chemistry and Chemical Engineering, Shandong University of Technology, Zibo 255000, P.R. China.*

[b] *Key Laboratory of Colloid and Interface Chemistry, Ministry of Education, School of Chemistry and Chemical Engineering, Shandong University, Jinan, 250100, P.R. China.*

[c] *School of Chemistry and Chemical Engineering, Hainan University, Haikou, 570228, P.R. China.*

* *Corresponding authors E-mail: yingchyan07@163.com (Y. Yan); yangjian@sdu.edu.cn (J. Yang)*

Experimental section

Materials. Tin beads (Sn, 3-5 mm, ＞99%) and Bismuth beads (Bi, 2-3 mm, ＞99%) are bought form Shanghai Macklin Biochemical Technology Co., Ltd. Multi-walled carbon nanotubes (MWCNT) is obtained from Nanjing XFNANO Materials Tech Co.,Ltd. Glycerol was ovtained from Aladdin Biochemical Technology Co., Ltd. As a comparative samples, tin powder (μ-Sn, 400 mesh), bismuth (μ-Bi, 200 mesh) was obtained from Aladdin Biochemical Technology Co., Ltd. And the commercial cathode of $Na_x[Ni_{1/3}Fe_{1/3}Mn_{1/3}]O_2$ (Na_xMO_2) was obtained from the market. The $Na_3V_2(PO_4)_3$ (NVP) was fabricated by sol-gel method according to previous work.[1]

Synthesis of SnBi/C. SnBi/C powder was synthesized via a thermally assisted ultrasonication process using a probe sonicator (Ymnl-1500Y, 650 W) under the power of 66%. Specifically, 4.3 g of Sn and 5.7 g of Bi were first heated in a muffle furnace (VBF‑1200X) at 300 °C for 3 h to obtain 10 g of molten metal alloy. Concurrently, 20 g of glycerol was pre‑heated to 150 °C in a beaker using an oil bath equipped with a hot plate. A designated amount of multi‑walled carbon nanotubes (MWCNTs) was then added to the glycerol and uniformly dispersed under ultrasonication. The MWCNT loading was varied as 0, 0.03, 0.06, 0.10, or 0.15 g per 10 g of molten alloy. The molten metal was subsequently poured into the resulting suspension. The ultrasonication step was performed under isothermal conditions at 170 °C for 30 min, with a pulsed cycle of 4 s on and 4 s off. After cooling, the product was washed three times each with deionized water and ethanol, followed by drying at 45 °C for 12 h to obtain the final SnBi/C material. As control samples, SnBi was obtained by directly physically mixing 0.43 g of Sn with 0.57 g of Bi, while SnBiC was prepared by directly physically mixing 0.43 g of Sn, 0.57 g of Bi, and 0.015 g of MWCNTs.

Materials characterizations

X-ray diffractometer (XRD) patterns were recorded on an XRD diffractometer (Bruker D8 Advanced, Germany), with mono-chromatic Cu kα as the radiation source (λ = 1.5418 Å). Scanning electron microscope (SEM) images and X-ray energy dispersive spectra (EDS) were obtained from a field-emission scanning electron microscope (ZEISS Gemini SEM 300, Germany). High-resolution transmission electron microscopy (HRTEM) images were acquired using JEOL JEM‑2100 transmission electron microscope (Japan). Raman spectra were recorded using an in situ UV confocal Raman spectrometer (LabRAM HR800, Horiba Jobin Yvon, Japan) with an excitation wavelength of 532 nm. The tap density was measured using a JZ-1 powder tap density tester with a drop height of 50 mm, a tapping count of 3000, and a tapping duration of 50 min.

Theoretical calculation details

The HOMO and LUMO calculations of the different molecules were performed using the Gaussian 16 package at B3LYP/6-311++G** level.[2] Additionally, the LUMOs of various functional groups were visualized using Visual Molecular Dynamics (VMD) software.[3]

Electrochemical measurements

All the electrochemical properties of were evaluated in CR2032-type coin cells. The anode was fabricated by mixing active materials, carbon black and binder in a weight ratio of 70:20:10 homogeneously with a trace of deionized water. In particular, due to the poor adhesion of poly(ethylene oxide) (PEO) binder to the current collector, 1 wt.% sodium polyacrylate is added to the slurry system when PEO is employed as the binder. The slurry was then spread on a clean copper foil by a doctor blade. After staying overnight in a vacuum oven at 60 ^oC, the foil was punched into discs with a diameter of 10 mm. The mass loading of the active material used for half-cell is found to be ~1.2-1.4 mg cm^{-2}. This working electrode was transferred to an Argon-filled glove box (Mikrouna, Super 1220/750/900, H_2O < 1 ppm, O_2 < 1 ppm) and assembled with a hand-made sodium foil as the counter and reference electrode, a Glassfiber (Whatman GF/F) as the separator, and 1.0 M $NaPF_6$ in diethylene glycol dimethyl ether (DGM) as the electrolyte together for half-cells. In full-cells, the commercial cathode of $Na_x[Ni_{1/3}Fe_{1/3}Mn_{1/3}]O_2$ (Na_xMO_2) was directly obtained with the mass loading of 12 mg cm^{-2}. While the home-made NVP materials was blended with carbon black and poly(vinylidenefluoride) in a weight ratio of 8:1:1, on an aluminum foil. The capacity ratio of the N/P was controlled to be 1:1.2. The electrolyte was 1.0 M $NaPF_6$ in DGM. Based on these cells, cyclic voltammetry (CV) curves were measured by an electrochemical workstation (Lanlike LK2005A, China) at room temperature. Galvanostatic discharge/charge voltage profiles were achieved by programmable battery cyclers (LAND CT2001A, China).

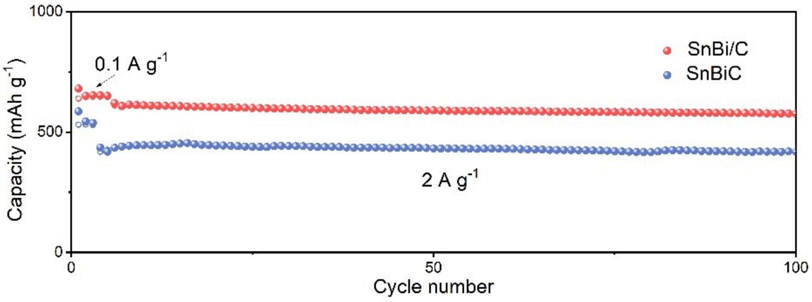

Figure S1. Cycling performances of SnBiC and SnBi/C.

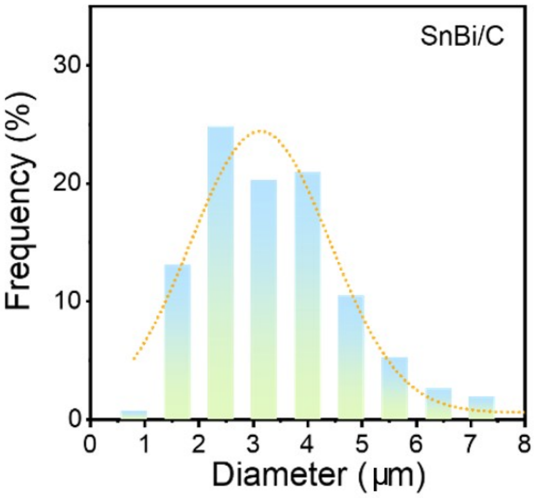

Figure S2. Particle size distribution of SnBi/C form the SEM image in the main text.

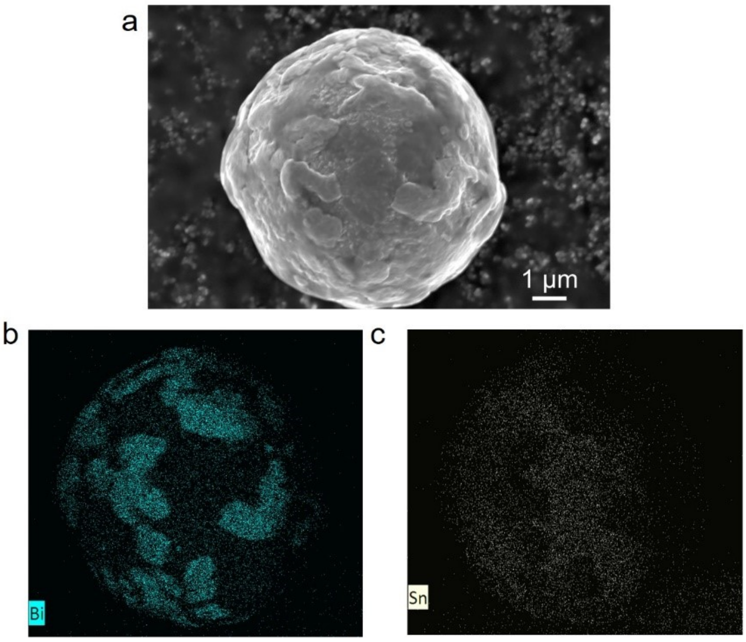

Figure S3. (a) SEM image and (b, c) elemental maps of Sn and Bi in SnBi-0. Here, SnBi-0 is prepared without the addition of MWCNT.

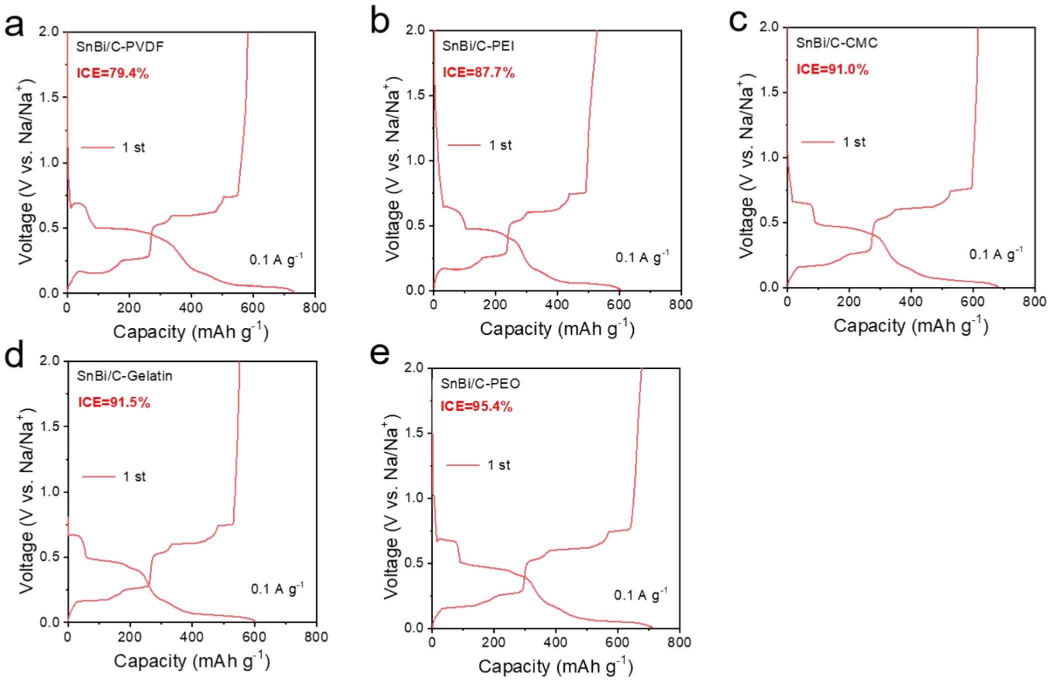

Figure S4. GCD voltage profiles of SnBi/C as binder with (a) PVDF, (b) PEI, (c) CMC, (d) Gelatin and (e) PEO as the binder.

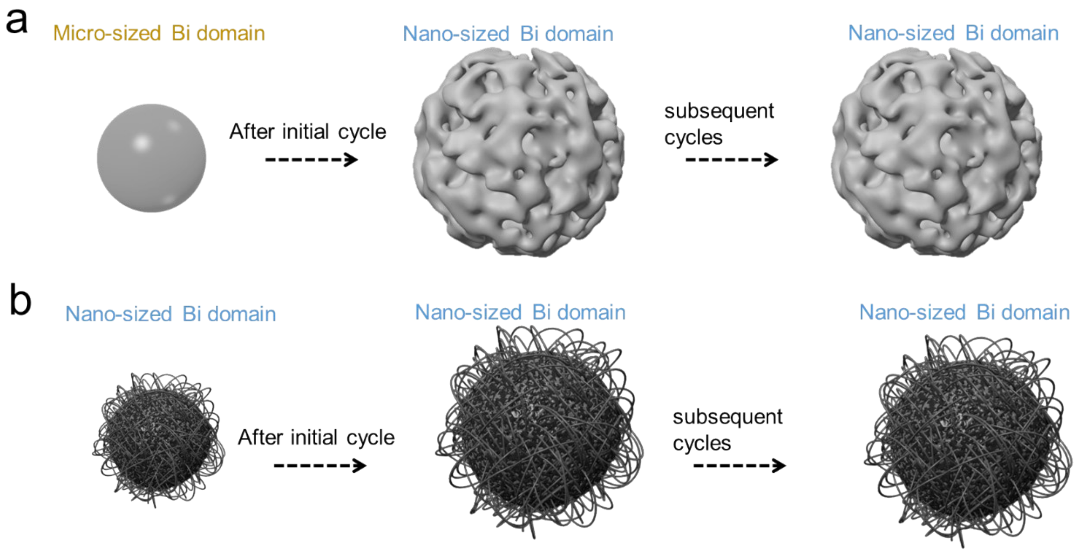

Figure S5. Schematic of the structural evolution of (a) bulk Bi and (b) SnBi/C during cycles.

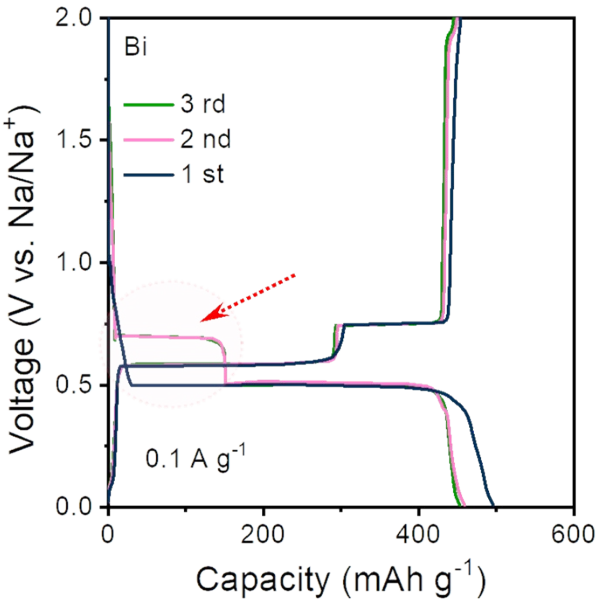

Figure S6. Initial three voltage profiles of micro-sized Bi bulk.

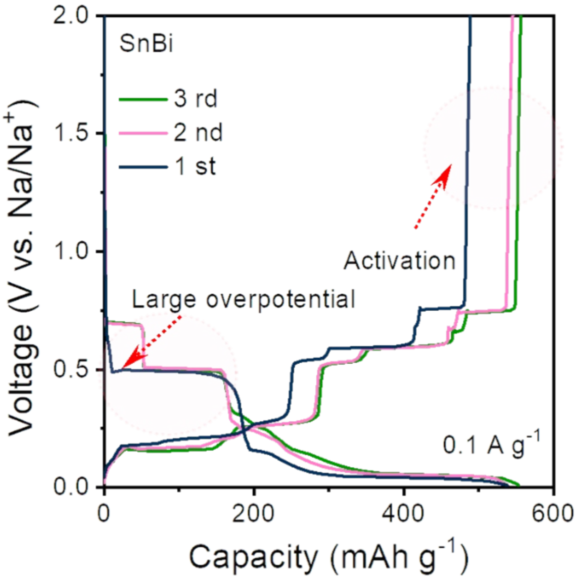

Figure S7. Initial three voltage profiles of SnBi.

The large over-potential of SnBi during the initial cycle is the primary reason for the decrease in its initial energy efficiency. In contrast, the two-stage mechanism of the Bi domain in SnBi/C not only helps alleviate the bulk volume change of the anodes but also contributes to improving the overall cycle energy efficiency.

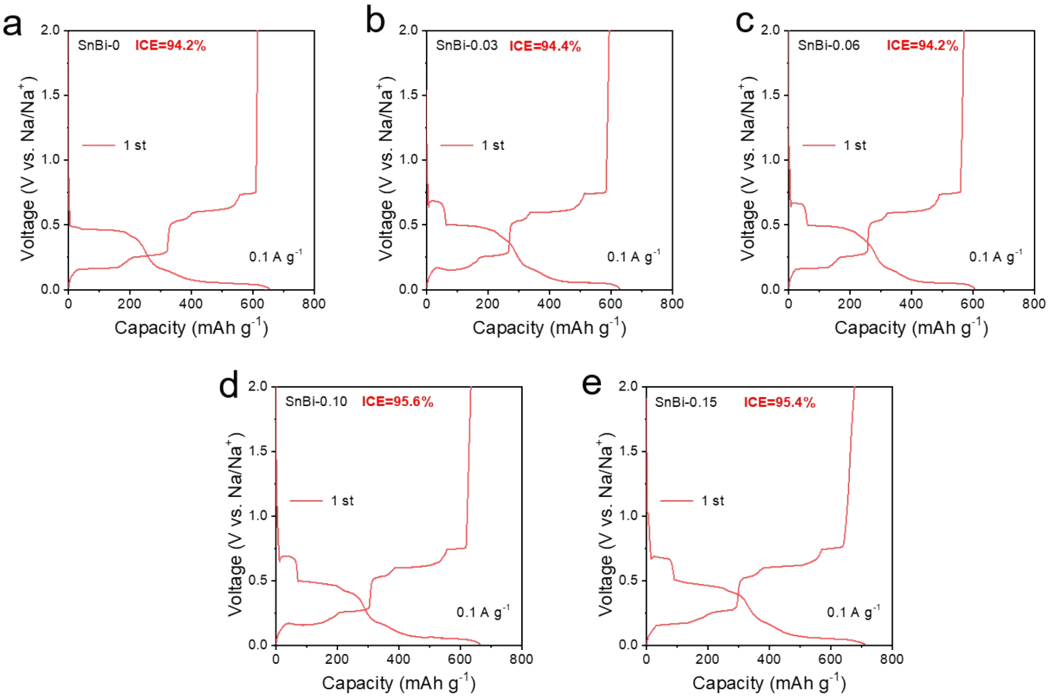

Figure S8. GCD voltage profiles of SnBi/C with (a) 0 g, (b) 0.03 g, (c) 0.06 g, (d) 0.10 g and (e) 0.15g MWCNT added per 10 g SnBi.

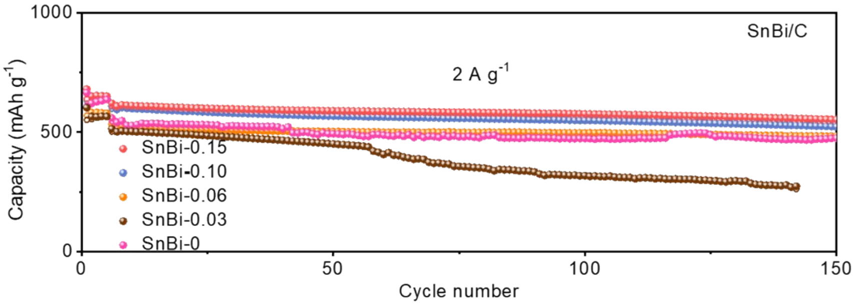

Figure S9. Long cycling performances of SnBi/C with 0 g, 0.03 g, 0.06 g, 0.10 g and 0.15 g MWCNT added per 10 g SnBi.

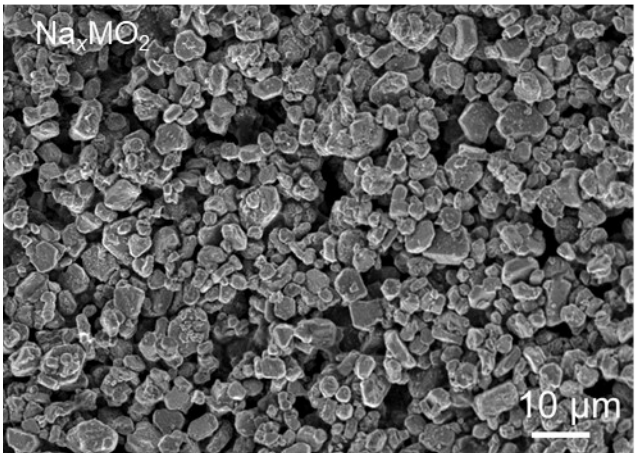

Figure S10. SEM image of commercial Na$_x$MO$_2$ electrode.

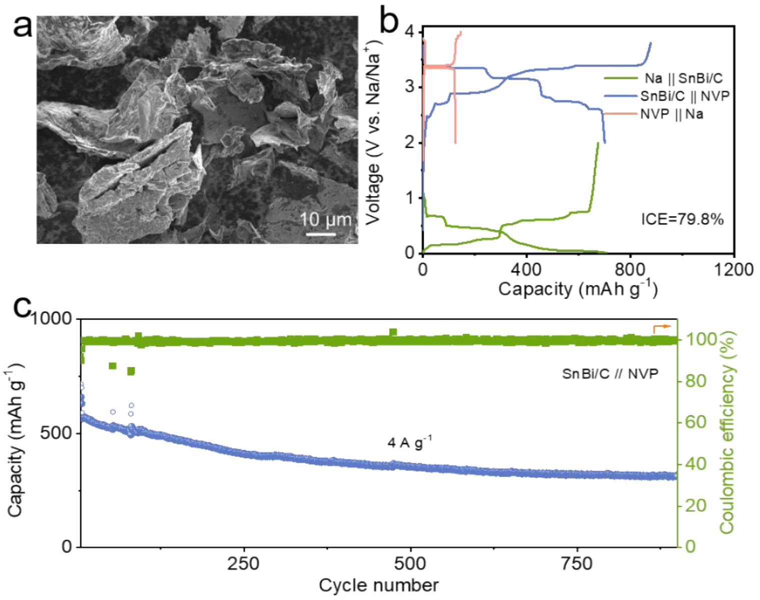

Figure S11. (a) SEM image of NVP. (b) Initial GCD voltage profiles of Na||SnBi/C, Na||NVP and SnBi/C||NVP. (c) The long-term cycling performance of SnBi/C||NVP.

The GCD voltage profile of SnBi/C||NVP shows the all the sodiation and de-sodiation stage of SnBi/C, so the high charge capacity of 876 mAh g^{-1} and discharge capacity of 700 mAh g^{-1} are obtained with the high ICE of 79.8% without any pre-sodiation process.

Table S1. Comparison of ICE and cycling stability of Sn, Bi, and various Sn/Bi binary composites in full-cells for sodium ion storage.

Anode	ICE (Full-cells)	Electrochemical performances (Current density, cycles, Capacity remained, (mAh g_{anode}^{-1}) (Full-cells)	Ref.
SnBi/C	86.2%	2 A g_{anode}^{-1}, 600, 493	This work
9226-SWCNT (Sn)	82.6%	0.2 A $g_{cathode}^{-1}$, 350, 94.69 mAh $g_{cathode}^{-1}$	4
nano-Bi@HC	Pre-sodiation	2 A g_{anode}^{-1}, 4000, ~390	5
Sn/Bi@C	Pre-sodiation	5 A g_{anode}^{-1}, 300, 457	6
BixSnSb@C	Pre-sodiation	50 mA $g_{cathode}^{-1}$, 100, ~90 mAh $g_{cathode}^{-1}$	7
Sn70Bi30	--	--	8
p-$Bi_{57}Sn_{43}$@C	~83%	0.6 A $g_{cathode}^{-1}$, 200, 83.4 mAh $g_{cathode}^{-1}$	9
dimer-like Sn-Bi@C	Pre-sodiation	2 A g_{anode}^{-1}, 300, 323	10
Bi/Sn@3D-C	--	--	11

References

1 Y. Xu, Q. Wei, C. Xu, Q. Li, Q. An, P. Zhang, J. Sheng, L. Zhou, L. Mai. *Adv. Energy Mater.*, 2016, **6**, 1600389.

2 Z. Ding, X. Long, C. Dou, J. Liu, L. Wang. *Chem. Sci.*, 2016, **7**, 6197-6202.

3 W. Humphrey, A. Dalke, K. Schulten. *Mol. Graph.*, 1996, **14**, 33-38.

4 Z. Chen, Y. Li, L. Wang, J. Zhang, R. Dang, H. Yu, B. Wang, C. Xu, H. Li, Y. Li, Y. Li, L. Zhou, F. Xie, R. Xiao, Y. Lu, H. Li, X. Huang, L. Chen and Y.-S. Hu, *Nat. Energy*, 2026, DOI: 10.1038/s41560-026-01974-2.

5 Z. Lu, H. Yu, Y. Wei, C. Cao, R. Liang, G. Cai, S. Jin, H. Jin, Y. Ni, Y. Lin and H. Ji, *J. Am. Chem. Soc.*, 2025, **147**, 28714-28722.

6 Y. H. Peng, Y. Y. Wang, Z. Y. Wang, G. S. Shao and B. H. Hou, *Adv. Funct. Mater.*, 2025, DOI: 10.1002/adfm.202513942.

7 J. Zhao, B. Liu, W. Yao and X. Ding, *J. Energy Storage*, 2024, **93**, 112407.

8 P. Gandharapu, A. Das, R. Tripathi, V. Srihari, H. K. Poswal and A. Mukhopadhyay, *ACS Appl. Mater. Interfaces*, 2023, **15**, 37504-37516.

9 J. B. Tian, S. G. Guo, B. Gao, M. Liu, Y. Zhou, J. W. Ren, M. Javanbakht, H. Omidvar, Z. Li, H. Song and K. F. Huo, *Sci. China Mater.*, 2025, **68**, 3646-3656.

10 X. Hou, Y. Zhu, Q. Yao, J. Song, C. Wang, Y. Zhou, S. Zeng, J. Yang and Y. Qian, *J. Energy Chem.*, 2023, **79**, 468-476.

11 H. Yang, L. Y. Yang, A. Abliz, S. Y. Wang, F. J. Zhao, M. Zhang, J. Li and H. B. Li, *Ionics*, 2021, **27**, 1429-1437.